ELSEVIER

Contents lists available at ScienceDirect

Tribology International

journal homepage: www.elsevier.com/locate/triboint



Friction and wear reduction by glycerol oleates: The molecular basis for performance variations in the presence of water and acetic acid

Inga Kicior ^{a,b}, Lauren Matthews ^{a,c}, Andrew J. Britton ^b, Elizabeth A. Willneff ^d, Camille Hammersley ^e, Ardian Morina ^e, Peter J. Dowding ^f, Veijo Honkimäki ^a, Sven L.M. Schroeder ^{b,g,*}

- ^a European Synchrotron Radiation Facility, 71 Av. des Martyrs, Grenoble 38043, France
- ^b School of Chemical and Process Engineering, University of Leeds, Leeds LS2 9JT, United Kingdom
- ^c ISIS Neutron and Muon Source, Rutherford Appleton Laboratory, Chilton OX11 0QX, United Kingdom
- d School of Design, University of Leeds, Leeds LS2 9JT, United Kingdom
- e School of Mechanical Engineering, University of Leeds, Leeds LS2 9JT, United Kingdom
- f Infineum UK Ltd., Milton Hill, Abingdon OX13 6BB, United Kingdom
- g Diamond Light Source, Harwell Science and Innovation Campus, Didcot OX11 ODE, United Kingdom

ARTICLE INFO

Keywords: Organic friction modifier Polar impurity Self-assembly Adsorption Wear Friction

ABSTRACT

Friction and wear reduction by pure and technical grade glycerol monooleates (GMOs) was investigated in commercial and model base oils, including the influence of water and acetic acid (AA) impurities. Small-angle X-ray scattering (SAXS) indicated they cause micelle swelling and elongation. AA reduces the separation of OFM from oil at room temperature (RT). Tribotests in a mini-traction machine with white light interferometry (WLI) show that OFMs decrease the traction coefficient, especially at higher temperatures. AA addition also lowered the traction coefficient at RT. X-ray photoelectron spectroscopy (XPS) revealed surface chemical changes that depend on both tribotest conditions and lubricant composition. Wear was associated with the oxidation of metallic iron. The effects of impurities intrinsic to technical GMO appeared to be significant.

1. Introduction

Lubricants ensure the smooth operation of engines by reducing friction and wear, cooling the system, and preventing corrosion [1,2]. Lubricant performance is an important factor in reducing energy wastage and greenhouse gas emissions [3,4]. Commercial lubricants are complex formulations that typically contain a package of additives dissolved or dispersed in a base oil. Additives include, for example, antioxidants, viscosity regulators, friction modifiers and anti-wear agents. Anti-wear additives, such as zinc dialkyl dithiophosphate (ZDDPs) or molybdenum dithiocarbamate (MoDTC), have been widely used since the 1940s and provide wear protection by forming tribolayers [5]. Degradation products of such additives contain sulphur and phosphorus compounds that can poison the catalytic converters in vehicles [6]. Moreover, from the perspective of electric vehicles, tribolayers increase energy consumption due to their resistance to electric currents [7]. Wear- and friction-reducing agents with better compatibility are therefore intensively studied, e.g. nanoparticles [8-11], polymers [12-16], oxide-based additives [17], ionic liquids [18–21], and organic friction modifiers (OFMs) [22–26]. OFMs are usually nonionic surfactants containing carbon, oxygen, hydrogen and nitrogen, built of a nonpolar tail with at least 12 carbon atoms and a polar head group [27]. Bio-derived OFMs are particularly attractive because of their sustainability, which includes not only a low carbon footprint but also less propensity to form noxious degradation products as a result of the absence of sulphur and phosphorus groups.

Friction reduction by OFMs is often assumed to stem from monolayer adsorption of the surfactant molecules to the interface, causing physical separation of the contact [3,22,27]. Therefore, most studies on OFM tribological performance focus on friction reduction in the boundary lubrication regime, where multiple asperity-asperity contacts occur. Due to their amphiphilic nature, OFMs also tend to form reverse micelles in nonpolar solvents like base oils [28–30]. There is a balance between self-assembly of micelles and adsorption. Adsorbed layers can indeed consist of reverse micelles or clusters of micelles, rather than a monomolecular layer [31,32]. An equilibrium model for bulk and interface

^{*} Corresponding author at: School of Chemical and Process Engineering, University of Leeds, Leeds LS2 9JT, United Kingdom. E-mail address: s.l.m.schroeder@leeds.ac.uk (S.L.M. Schroeder).

aggregation has therefore been proposed [33].

In a tribological contact, the molecular structure and composition of OFM films can be changed, e.g. resulting in multilayer film formation or tribochemical reactions in hotpots with high temperature and/or pressure. Moreover, small amounts of polar molecules such as water, alcohols or acids can enter the lubricant from the environment and cause the chemical transformations of lubricant components. Such impurities can not only influence the self-assembly and adsorption processes but also create the potential for reactions with other components in the oil phase, including metal particles released by wear. Such effects modulate, often synergistically, the tribological performance of the lubricant [34,35]. Especially water and acids are usually detrimental to lubrication, causing enhanced wear and corrosion [36]. Their presence is inevitable under practical conditions, especially so with the increasing use of biofuels, which are glycerol esters of fatty acids [37]. It is therefore desirable to understand the molecular basis for the effects of polar molecules, acetic acid and water, on the structure and performance of OFMs.

In this study, we aimed to determine the mechanism of friction reduction of the chosen OFMs, namely glycerol monooleate (GMO, a single-component, model OFM) and technical grade GMO (industrially used mixture with glycerol di- and trioleate), in the model lubricants based on *n*-dodecane in the absence and presence of polar molecules: acetic acid and water by comparison of their tribological performance and colloidal self-assembly. The tribological characterization of the systems was performed with a mini-traction machine (MTM). The morphology and chemical composition of the steel surfaces were characterized by white light interferometry (WLI) and X-ray photoelectron spectroscopy (XPS), respectively. Colloidal self-assembly in the model lubricants was examined by small-angle X-ray scattering (SAXS).

2. Experimental

2.1. Materials

GMO – glycerol monooleate (1-oleoyl-rac-glycerol, \geq 99 %, Sigma Aldrich, see Fig. 1a), and technical GMO – a technical mixture of glycerol mono-, di- and trioleate (1-oleoyl-rac-glycerol, \sim 40 %, Sigma Aldrich, see Fig. 1b) were used as organic friction modifiers (OFMs). GMO was stored below 0°C. Yubase-4 (group III mineral oil, SK Lubricants; kinematic viscosity at 40°C: 19.57 cSt, viscosity index: 122) and model oil n-dodecane (>99 %, Sigma Aldrich; kinematic viscosity at 25°C: 1.8 cSt) were used as base oils (BOs). Milli-Q deionized water (resistivity: 18.2 M Ω -cm) and acetic acid (\geq 99 %, Sigma Aldrich) were used to study the effect of polar components. Heptane (\geq 99.9 %, Sigma Aldrich), acetone (>99 %, Sigma Aldrich) and ethanol were used for cleaning. All chemicals were used without further purification.

20 mM (0.02 M) single-OFM solutions were prepared by mixing OFM with base oil and magnetic stirring of the resulting mixture for at least 30 min at 60°C. The resulting solution was used as soon as possible after cooling down to ambient temperature. Model lubricants with polar components were prepared similarly, by adding the desired amount of water or acetic acid (AA) with the OFM. Water content was set to 1:5 OFM:water molar ratio, resulting in 100 mM (0.1 M) water concentration. For AA, two OFM:AA molar ratios were examined: 1:5 and 1:10, resulting in 100 mM (0.1 M) and 200 mM (0.2 M) AA concentrations, respectively. Such high concentrations of additives and polar molecules (~ 1 wt% OFM, 0.2 wt% water, ~ 2.7 wt% and ~ 5 wt% for 0.1 M and 0.2 M AA, respectively) were chosen to ensure that species could be detected by the X-ray analytical measurements, in which the solute/solvent contrast, especially at high photon energies, is low and cannot be enhanced by, e.g., deuteration of the components as practiced in neutron

Fig. 1. Chemical structures of OFMs used in this study: a) glycerol monooleate (GMO), b) technical GMO as a mixture of (1) glycerol monooleate, (2) glycerol dioleate and (3) glycerol triolate.

analysis.

Mini-traction machine (MTM) standard specimens, 46 mm diameter discs and 19.05 mm ($\frac{3}{4}$ ") balls, were purchased from PCS Instruments. Both discs and balls are made of highly polished AISI 52100 bearing steel, with the composition presented in Table 1. Properties of the specimens are shown in Table 2. Before a tribotest, the ball and the disc were cleaned in an acetone ultrasonic bath for 20 min. For each test, 35 ml of lubricant was used to ensure full immersion of the disc and ball contact.

2.2. Methods

2.2.1. Mini-Traction Machine (MTM)

Friction and wear performance testing was conducted with an MTM-2 instrument (PCS Instruments, United Kingdom). This instrument implements a ball-on-disc geometry with the disc and ball specimens described above. Our investigations of lubricant performance focused on high values of the slide-to-roll ratio (SRR), which is defined as the ratio of the sliding speed $u_{\rm S}$ to the entrainment speed $U_{\rm S}$, where mostly sliding prevails at the contact. The SRR relates to the speeds of the ball and disk surfaces $u_{\rm B}$ and $u_{\rm D}$, respectively, through

$$SRR = \frac{u_s}{U} = \frac{|u_D - u_B|}{U} = \frac{|u_D - u_B|}{\frac{1}{2}(u_D + u_B)}.$$
 (1)

The maximum SRR is 200 %, which represents the condition of 'pure sliding', when either u_B or u_D are 0. When u_b is zero, a wear track is created on the disc. The SRR is zero when the ball and disc rotate with the same speed in the same direction, representing the condition of 'pure rolling'. When the ball and surface rotate at different finite speeds relative to each other at the contact, then mixed sliding-rolling conditions apply.

The conditions of the tribotests run for OFM solutions in Yubase-4 were similar to those used by Campen *et al.* [22]. The same set of conditions was unsuitable for the model formulations in *n*-dodecane because of its lower viscosity. For Yubase-4, it was possible to run tests in which SRR, speeds and temperature were kept constant for 2 h (timed step), followed by a Stribeck analysis as a function of entrainment speed at constant temperature and SRR. For the samples based on *n*-dodecane, only Stribeck curves could be measured due to excessive friction at the timed step test speed that forced the premature end of the procedure. Details of the conditions are collated in Table 3

For the tests in Yubase-4, only base oil and OFM solutions without polar components were measured to obtain a preliminary set of data for a more realistic system (prolonged constant friction at elevated temperature and commercial base oil) and to compare if the same trends for friction reduction are noticed for the model system with n-dodecane. For formulation in n-dodecane tests were performed at least twice for a reproducibility check, although some of the tests (especially at 25° C) were not found to vary significantly across different formulations, suggesting high reproducibility. These were therefore performed only once. Generally, where changes were observed, the observation of monotonic trends across different measurements also indicates good reproducibility. The full list of examined formulations is presented in Table 4

2.2.2. X-ray Photoelectron Spectroscopy (XPS)

XPS measurements of the discs after tribotesting were performed in an EnviroESCA near-ambient pressure system (Specs Surface Nano Analysis, Germany) with a monochromated Al K_{α} X-ray source (photon energy: 1486.6 eV). The diameter of the beam spot on the sample

Table 2Properties of the MTM standard specimens.

Specimen	Diameter (mm)	Roughness, R_q (nm)	Elastic modulus (GPa)	Poisson's ratio	Hardness (HV)
Disc	46	10	210	0.29	720–780
Ball	19.05	20	210	0.29	800-920
	(3/4")				

Table 3
Tribotest conditions.

Parameter	Yubase-4	n-dodecane
Temperature	60°C and 100°C	25°C and 55°C
Load (contact pressure)	40 N (1 GPa)	20 N (0.85 GPa)
SRR	$200 \% (u_b = 0)$	150 %
Recipe	2 h timed step followed by Stribeck	Stribeck only
U (Stribeck)	3000–15 mm/s	2500-25 mm/s
Speed (timed step)	20 mm/s	-
Test duration (timed step)	2 h	-

Table 4Tested formulations. LT and HT mean lower and higher temperatures, respectively, for the specific test (60°C and 100°C for Yubase-4, 25°C and 55°C for *n*-dodecane).

#	OFM	Yubase-4	n-dodecane
1	None	LT, HT	LT, HT
2	None + polar molecules	-	100 mM water LT, HT 100 mM acetic acid LT, HT
3	GMO	LT, HT	LT, HT
4	GMO + polar molecules	-	100 mM water LT, HT 200 mM acetic acid LT, HT
5	Tech. GMO	LT	LT, HT
6	Tech. GMO $+$ polar molecules	-	100 mM water LT, HT 100 mM acetic acid LT, HT 200 mM acetic acid LT, HT

surface was ca. 0.3 mm. Measurements were performed under high vacuum conditions, with pressures approximately in the 10^{-5} mbar range.

To protect the steel surface from air after the MTM tests, the steel discs were kept covered in the lubricant oil film until XPS measurements were performed. The excess lubricant was then removed by rinsing with heptane and gently wiping with a fresh Kimwipe tissue, followed by blowing with air to remove dust. For each XPS run, 3 discs were placed on the sample stage and fixed with a small piece of double-sided conductive tape.

C 1 s, O 1 s and Fe 2p core level emission spectra were recorded as an average of 4 scans with a pass energy of 50 eV, 0.1 eV step size and 0.2 s dwell time per datapoint. The footprint of the X-ray beam on the sample is approximately a circle with a diameter of 300 μm . For each sample, XPS measurements were performed inside the wear track formed during the MTM test and $\it ca.\,1.5$ mm away from the track to assess tribochemical changes from purely surface chemical changes induced by contact with the lubricant.

Data analysis of the collected spectra was performed with CasaXPS software, using Shirley backgrounds and Gaussian-Lorentzian line shapes (70 % Gaussian) for all emission lines except for the metallic ${\rm Fe}^0$ 2p_{3/2} line, which was fitted with a Lorentzian asymmetric line shape LA

Table 1
Chemical composition of AISI 52100 steel [38].

С	Cr	Mn	P	Si	S	Fe
0.98–1.10 %	1.30–1.60 %	0.25-0.45 %	\leq 0.025 %	0.15-0.30 %	0.03 %	bal.

(1.2,4.8,3) [39,40]. The binding energy scale was calibrated using the centroid of the aliphatic C 1 s emission peak component at 285.0 eV. Fe 2p spectra exhibit not only the familiar 2p spin-orbit split but also complex multiplet effects, hence the common practice [39–42] of analysing only the Fe $2p_{3/2}$ component was followed.

2.2.3. White Light Interferometry (WLI)

Variations in the morphology of the wear tracks between different samples were visible by the unaided eye. To obtain accurate 3D surface profiles of the worn discs, non-destructive white light interferometry (WLI) measurements were performed using the NPFLEX-1000 (Bruker, Germany) instrument. Calibration verification was undertaken using a 10.08 $\,\mu m$ step height standard. Samples after XPS measurements (without residual oil film) were scanned at 4 points, evenly distributed around the sample surface to ensure repeatability. The resulting $300\times300~\mu m$ profiles with the wear track around the middle of the picture were analysed using Bruker Vision64 software to obtain wear track width. 3D image processing was performed to flatten the measured surface and obtain roughness values after the application of the Gaussian regression filter.

2.2.4. Small-Angle X-ray Scattering (SAXS)

SAXS measurements of doped and undoped OFM solutions in n-dodecane were performed at the ID02 TRUSAXS beamline at the European Synchrotron Radiation Facility (Grenoble, France). Three sample-to-detector distances were used (1, 10, 31 m), combined with an X-ray energy of 12.23 keV ($\lambda=0.101$ nm), leading to an available q-range of 0.001-7.6 nm $^{-1}$ (0.0001-0.76 Å $^{-1}$), where q is the scattering vector,

$$q = \frac{4\pi \sin\theta}{\epsilon^2},\tag{2}$$

with θ being the scattering angle. SAXS measurements were performed in a flow-through capillary with OD = 2 mm with automatic washing using Hellmanex and water. Data were collected using an Eiger2 4 M detector (Dectris, Switzerland) pixel array detector and sample transmission was measured simultaneously. Samples underwent an irradiation test to ensure the exposure time ($t_{\rm exp}=0.1$ s) caused no damage, then a scan along the capillary of 10×0.1 s measurements was taken and averaged to improve data quality. Then, the 2D data underwent reduction: normalisation to an absolute intensity scale, azimuthal integration, and corresponding background subtraction to yield the 1D SAXS profiles expressed as I(q). Further details on the data analysis are included in the Supplementary Information equations 4-7.

3. Results and Discussion

3.1. Tribological Behaviour of the Model OFM Formulations

3.1.1. Effect of Base Oil - Yubase-4 vs. n-Dodecane

Yubase-4 is a commercially used base oil with a higher viscosity than n-dodecane, allowing for lubrication at higher temperatures, loads and slide-to-roll ratios (SRRs). Because it is a commercial mineral oil with variable composition, including molecules potentially adsorbing to the surface [43], it is more difficult to establish molecular structure/performance relationships for its formulations. Therefore, *n*-dodecane was predominantly used as a model base oil, building on previous studies by neutron techniques and with custom-built tribometers [44, 45]. An advantage of *n*-dodecane is also that it is liquid at room temperature and requires no additional heating to perform measurements. Solutions of OFMs in *n*-dodecane are clear and stable at room temperature, while OFM solutions in Yubase-4 are clear at the preparation temperature (60°C) but become cloudy at room temperature. The cloudiness arises from the additive precipitating out in the form of a powder or gel gathering further at the bottom of the container. Additionally, the lower viscosity of n-dodecane allowed for less vigorous

experimental conditions (*e.g.* lower temperature and SRR) to be used; using the same conditions as for Yubase-4 testing was not possible due to excessive wear, leading to the premature end of the measurement.

For both base oils, it was found that at the lower test temperature, the OFM additive does not affect the traction coefficient strongly as a function of time and speed; friction variations due to the OFM additive are observed at the higher test temperature. This suggests that at the lower test temperature the base oil film persists and carries the load, while at the higher temperature, the film breaks up as a result of the viscosity drop and the surface is protected only by adsorbed additive, if present. Higher temperature also ensures better solubilisation of the OFM, while at the lower temperature, some aggregates may remain in the oil, limiting the amount of the additive that can adsorb to the surface.

Without any additive, excessive wear prevented the timed step from finishing (Fig. 3b, Yubase-4 at 100°C), and the traction coefficient started rising dramatically from a value of 0.08 at ca. 100 mm/s entrainment speed to 0.165 at 15 mm/s (Fig. 2b, Yubase-4 at 100°C). Despite the substantial viscosity difference between Yubase-4 and ndodecane, the lambda ratio calculations (included in Supplementary Information Table S1) show that for both base oils at both test temperatures, the lambda ratio is much below 1 at the slowest entrainment speeds (15 mm/s for Yubase-4 and 25 mm/s for n-dodecane), which confirms the boundary lubrication regime, in which OFMs are supposed to operate generally. At higher entrainment speeds, the systems lubricated with n-dodecane and Yubase-4 at 100°C enter the mixed lubrication regime, and those lubricated with Yubase-4 at 60°C can reach the elastohydrodynamic lubrication regime. Temperature- and additiverelated trends remain the same for all base oils, as well as the maximum traction coefficient (ca. 0.14–0.16), even if the test conditions were different (temperatures, load, SRR, Stribeck curve measurement after the timed step or done on the fresh oil). Considering the similarity of results obtained in other OFM studies with n-dodecane [44,45] and with n-hexadecane (the latter at elevated temperature) [22,27,46], it is justified to use n-dodecane as a model base oil in tribological and structural studies.

3.1.2. Effect of OFM presence and type

Adding an OFM to the base oil leads to traction coefficient reduction. For formulations in Yubase-4, the effect on the Stribeck curve is well visible at 100° C (Fig. 2). For 2-hour tests carried out with Yubase-4, adding OFM reduces the traction coefficient at a given temperature (Fig. 3). Technical GMO shows the highest reduction of traction coefficient for tests in Yubase-4 at 60° C (Fig. 2a) and undoped and water-doped n-dodecane at 55° C (Fig. 4b, d) in the studied speed range. As tech. GMO is a mixture of around 40° GMO, 15– 40° glycerol dioleate and 15– 40° glycerol trioleate, the components with more oleyl chains are important in the friction reduction mechanism of this OFM, even if they have fewer free hydroxyl groups, mainly responsible for adsorption.

At 25°C, Stribeck curves for OFM-containing formulations in ndodecane have similar values to those of the base oil only, emphasizing the predominant influence of the base oil rather than OFM at this temperature. Between 25 and 55°C, the dynamic viscosity of n-dodecane drops from 1.344 mPa·s to ca. 0.920 mPa·s, resulting in a thinner lubrication film. Campen et al. [22] noticed similar trends between lower and higher test temperatures (35 and 100 $^{\circ}\text{C})$ for formulations in hexadecane, explaining that despite falling in mostly in the boundary lubrication regime (according to e.g. Hamrock and Dowson [47] or Chittenden et al. [48] models), the friction tests must have been carried out rather in a mixed lubrication regime, where the fluid film is not negligible. The lambda ratio calculated for *n*-dodecane at 25°C remains below 1 for entrainment speeds 25–1675 mm/s (boundary lubrication regime). At higher speeds, it enters the mixed lubrication regime, reaching the value of 1.372 at the maximum entrainment speed of 2500 mm/s. At 55°C, the lambda ratio remains below 1 for almost the

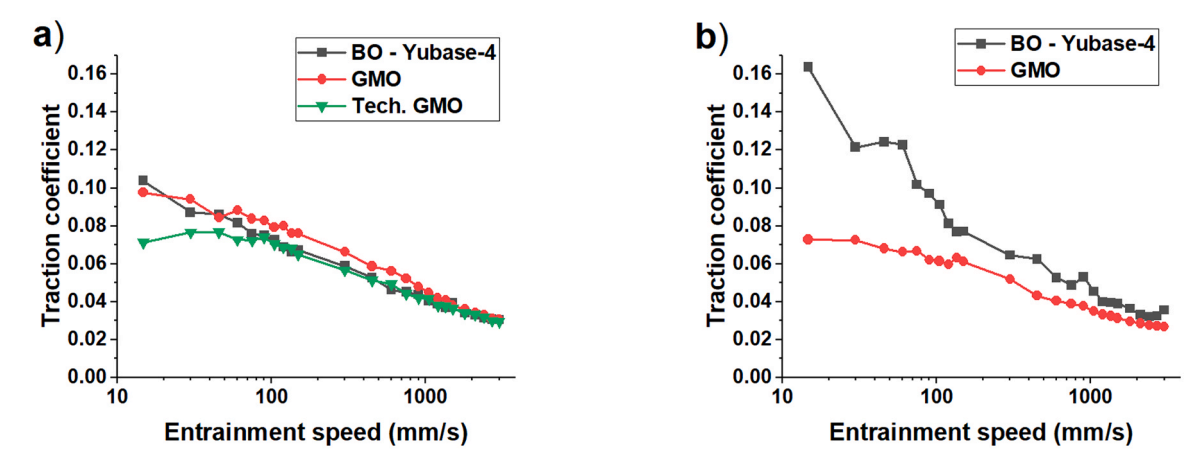


Fig. 2. Stribeck curves for OFMs in the Yubase-4 base oil after 2 h MTM testing at load 40 N, SRR= 200 %, at a) 60°C and b) 100°C. GMO lubricant at 100°C and tech. GMO at 60°C had the lowest traction coefficients, which were similar, especially at the lowest rolling speed (the thinnest lubrication film); tech. GMO was not tested at 100°C. The traction Stribeck curves generally converge at the highest rolling speeds (the first measurement point).

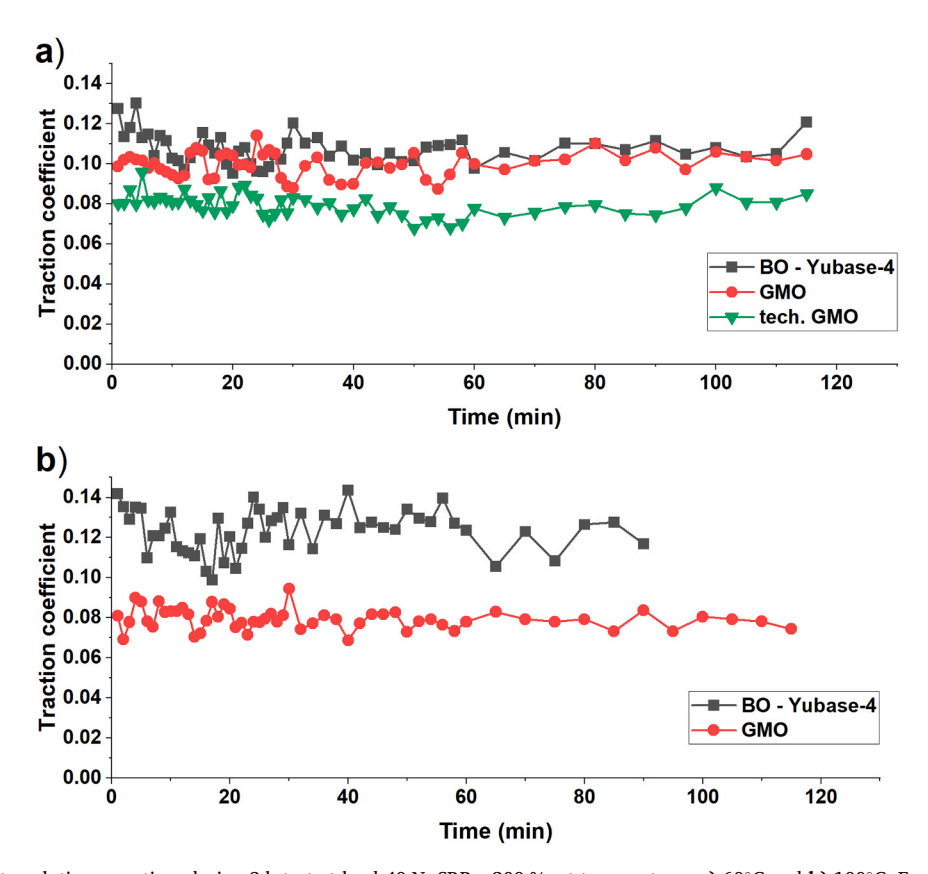


Fig. 3. Traction coefficient evolution over time during 2 h test at load 40 N, SRR= 200 %, at temperatures a) 60° C and b) 100° C. For most of the single-additive lubricants at both temperatures, the traction coefficient remains relatively stable during the test, apart from the base oil at 100° C for which the traction was the highest and the test was stopped prematurely due to excessive wear. The behaviour of GMO at 100° C and tech. GMO at 60° C is very similar.

whole speed range, and reaches 1.060 at 2500 mm/s. Increasing the temperature reduces the viscosity, leading to the fluid film breaking and more pronounced asperity-asperity contact. For lubricants with Yubase-4 (Fig. 3), the traction coefficient remains relatively constant over time for most of the samples at both temperatures. A significantly lower traction coefficient at 60° C for tech. GMO stands out compared to other lubricants at this temperature. At 100° C, the test with base oil only was stopped prematurely due to traction transducer readings out of the calibrated range – the traction coefficient is higher than OFM-containing formulations from the beginning of the test and slightly decreases before the forced end. The reasons are the wear of the specimens and the

lubricant film rupture, leading to inappropriate transducer readings in the final part of the test. The additive decreases traction and wear enough to complete the test.

3.1.3. Effect of Small Polar Molecules: Water and Acetic Acid

Water has a limited effect on the Stribeck curve shape for samples tested in OFM-containing oils at both studied temperatures (Fig. 4c and d). Only a mixture of base oil with water shows a significant difference compared to neat base oil. At $25^{\circ}C$, it presents a lower traction coefficient at faster rolling speeds and suddenly increases to the highest value from all water-doped formulations. At $55^{\circ}C$, the traction coefficient

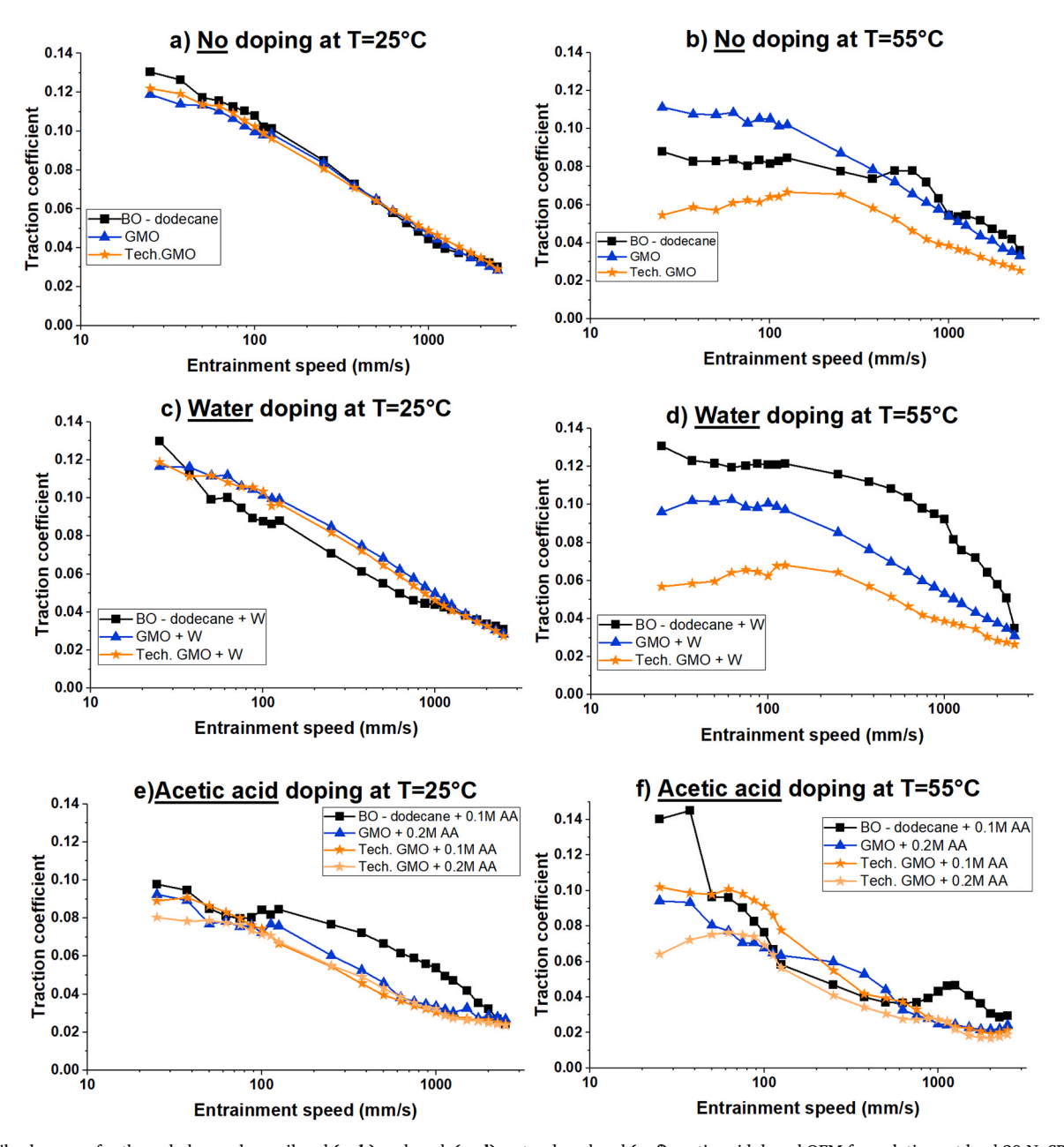


Fig. 4. Stribeck curves for the *n*-dodecane base oil and **(a, b)** undoped, **(c, d)** water doped and **(e, f)** acetic acid doped OFM formulations at load 20 N, SRR= 150 % and temperature **(a, d, e)** 25°C and **(b, e, f)** 55°C. Acid doping significantly affects the Stribeck curve evolution, contrary to water doping, which shows very similar behaviour to undoped systems.

remains high for almost the whole speed range. For OFM solutions, the Stribeck curves look very similar for undoped and water-doped systems (Fig. 4a-d; these subplots are collated in Fig. S1 in Supplementary Information), and the values of the traction coefficients at 25 mm/s entrainment speed are also comparable (Fig. 5). There is a slight traction coefficient reduction at the low entrainment speeds for the test with GMO + water at 55 °C compared to GMO only (Fig. 4bc and Fig. S1). The effect of water addition can be explained by the high polarity of water compared to nonpolar n-dodecane and their immiscibility. The added water is not dispersed in the oil and instead forms large droplets to reduce unfavourable contact between the water and oil. In this case, water could adsorb to the polar steel surface, creating an island of water rather than a uniform film. The addition of a surfactant (OFM) helps to transfer the water to the steel surface by entrapment of water inside the micelles. Therefore, the OFM is mainly responsible for friction reduction but water creates a layer between steel and the OFM. As pure GMO has

more free hydroxyl groups at the same concentration compared to tech. GMO, the water layer on the steel surface can facilitate the adsorption and friction reduction of GMO in the most boundary lubrication conditions. Yi et al. [26] proved that in MD simulation, and their reciprocating friction test on $\mathrm{Si}_3\mathrm{N}_4$ showed that environment humidity up to 30 % does not affect friction, compared to 0 % humidity; this can explain the very limited changes in Stribeck curves between water-containing and water-free formulations in this study. Although the effect may be present at higher water concentrations, adding this polar agent also reduces the solubility of OFMs and the stability of the lubricant at room temperature. Pure GMO is prone to precipitation, especially when water is added. Tech. GMO remains stable in the oil even in the presence of water. All the OFM formulations in n-dodecane form clear solutions at $55^{\circ}\mathrm{C}$ but due to the limited stability at room temperature, other water concentrations were not studied here.

The effect of AA is more complex than that of water. All the studied

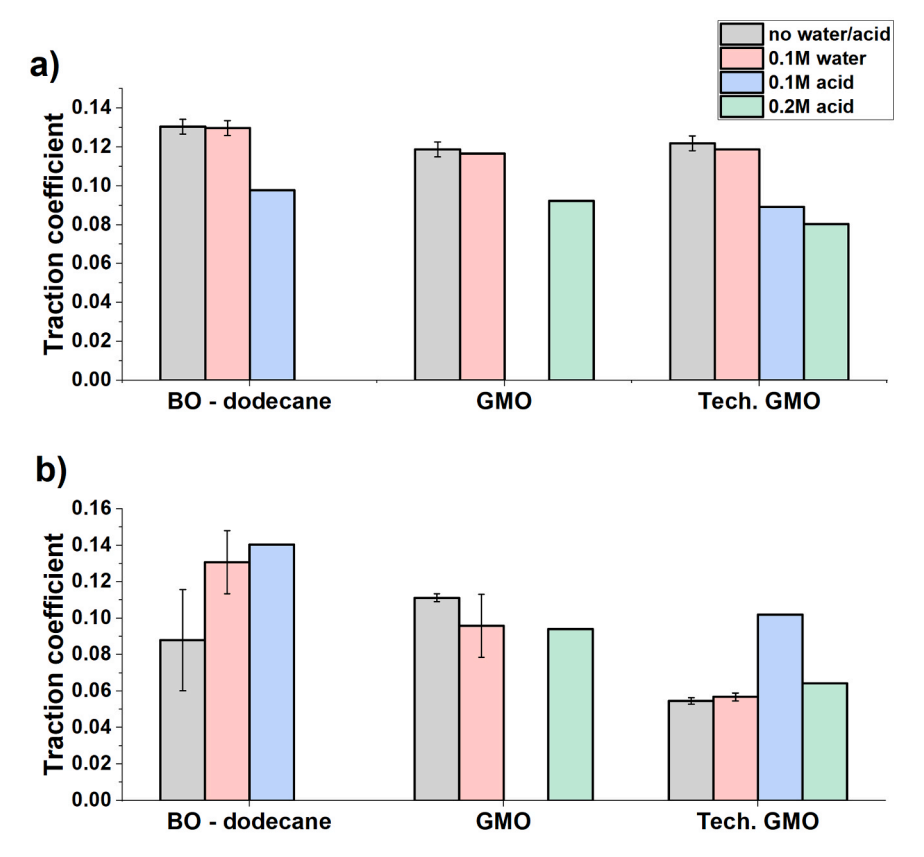


Fig. 5. Bar plots comparing traction coefficient for formulations at 25 mm/s entrainment speed (the slowest for the test) at a) 25°C and b) 55°C.

acid-containing formulations show a decrease in traction coefficient over the whole Stribeck curve at 25°C, and the difference between the base oil with AA only and oils with OFM is more pronounced than in all other cases of lubricants tested at lower temperature (both for Yubase-4 and n-dodecane-based lubricants). Also, as mentioned above, the Stribeck curves of formulations are very similar at this temperature in the presence and absence of water. GMO and tech. GMO solutions containing 0.2 M AA behave almost identically, and the traction coefficient is lower than for base oil + 0.1 M AA. At 55°C, most of the samples show similar levels of traction coefficient in high and medium rolling speeds, and more severe differences are observed at lower speeds (i.e. thinner lubrication films). In this case tech. GMO + 0.2 M AA exhibit the most efficient friction reduction in the low-speed range (ca. 25–55 mm/s). Surprisingly, the abnormal increase of the traction coefficient was noticed for tech. GMO + 0.1 M AA at 55°C (Fig. 5b), not following the decreasing trend with increasing acid concentration at 25°C (Fig. 5a). The traction coefficient for tech. $GMO + 0.2 M AA 55^{\circ}C$ is also slightly higher than undoped tech. GMO at the same temperature. Carboxylic acids are more soluble in alkanes than water, so acid-containing solutions are noticeably more stable at room temperature and do not show precipitation tendencies like water-containing ones. Nevertheless, changes in tribological behaviour suggest that the acetic acid plays an active role in the lubrication; the effect at 25°C can be explained by acid dissolution in *n*-dodecane, which appears to lead to better lubrication of the steel contact than by neat n-dodecane. Overall, n-dodecane with some AA content appears to be a more suitable solvent for OFMs. A similar approach of mixing alkanes with short carboxylic acids is adapted in e.g. chromatography to adjust the polarity of the eluent and consequently the solubility of the studied phases [49,50]. On the other hand, high corrosion around the wear track for tech. GMO + 0.2 M AA at 25°C suggests that the steel surface is attacked by the acid. X-ray reflectivity and MD simulations demonstrated that the water dopant adsorbs to the iron oxide surface before the OFM [44]. This can be

assumed for acetic acid as well, because of its polarity similar to water (dipole moment of 1.76 D for AA [51] and 1.85 D for water [52]). An adsorbed acid layer can promote better adsorption of the OFM onto the surface, protecting the contact and effectively reducing friction. A decrease of traction coefficient for base oil + 0.1 M AA at 25 $^{\circ}$ C can be interpreted as acetic acid working as a simple organic friction modifier, despite being a small molecule. However, for the alloy used in this study (standard bearing steel without anticorrosion alloy additives) the corrosion by AA is uncontrollable. Despite low friction, the wear can be severe and eventually, the high acid concentration is more damaging to the steel than AA-free base oil formulations. 0.1 M AA content substantially increased friction at the lowest speed compared to AA-free formulations at 55°C (Fig. 5b) which highlights the importance of both the nature of the small molecule polar additive and its concentration for the friction reduction properties of the oil. Elevated temperature prevents acid and OFM adsorption [53] onto the surface to the point that the additive cannot provide friction reduction. However, higher temperature can promote dissociative chemisorption [54]. Wang et al. [54] determined that strong chemisorption becomes an important factor from ca. 110°C, so it is not expected under the conditions used in the present study, where the maximum test temperature in n-dodecane was 55°C. However, the low viscosity of the *n*-alkane (as opposed to poly-alpha olefin in the previous study) may facilitate strong chemisorptive interactions (and other tribochemical reactions) at lower temperature. Concerning corrosion, normally, corrosion rates would increase at elevated temperatures in the presence of acetic acid. However, less rust or wear was noticed for tech. GMO + 0.2 M AA at 55°C compared to 25°C, which also confirms the importance of acid adsorption on the tribological performance and its decrease with increasing temperature.

3.2. Chemical and Morphological Changes of the Worn Surface

During the tribotests, values of the traction coefficient and the shape

of the Stribeck curve differ between tests depending on the lubricant formulation used and the temperature of the test. Directly from the test, information about the friction (between the surfaces) can be obtained. This is not possible for characterizing wear, so other techniques must be included to measure the wear track width and chemical change of the surface. Moreover, the OFMs can physisorb or chemisorb to the surface depending on the temperature [54]. Each disc sample after the test was examined by the naked eye. Substantial damage of the sample with visible corrosion was noted for the disc lubricated with tech. GMO + 0.2 M AA at 25°C, while it reached the lowest traction coefficient in the slow rolling speed from all measurements at 25°C. XPS measurements were conducted to get a better understanding of the processes of wear on the steel surface and possible attack of the polar small molecules promoting the (tribo)corrosion. Survey spectra of the discs (an example of an untreated reference sample is presented in Fig. 6a) showed distinct emission lines for iron (mainly Fe 2p), oxygen O 1 s and carbon C 1 s, as expected from the study of AISI 52100 steel composition (Table 1). A weak peak for calcium can be noticed around a binding energy of 350 eV and is an impurity in the steel.

C 1 s spectra of all measured samples (an example is presented in Fig. 6b) reveal adventitious carbon contamination on the disc from the cleaning process with heptane and residuals of the lubricant (for the untreated sample, the adventitious carbon comes mostly from the cleaning). As the wear tracks on various samples had visibly different depths and general morphology, the amount of residual oil is not constant. Trends in the concentration of specific carbon species are not clear. The main carbon species that can be distinguished are aliphatic carbon (C-C, C-H; used for binding energy scale calibration) and carbonoxygen moieties (C-OH, C-O-C, O-C=O) [55]. The additional peak at lower binding energy from the main peak ($BE \sim 284.8 \text{ eV}$) corresponds to C from iron carbide, which is present in the AISI 52100 microstructure in the form of distinct precipitates, separated from each other by even 5

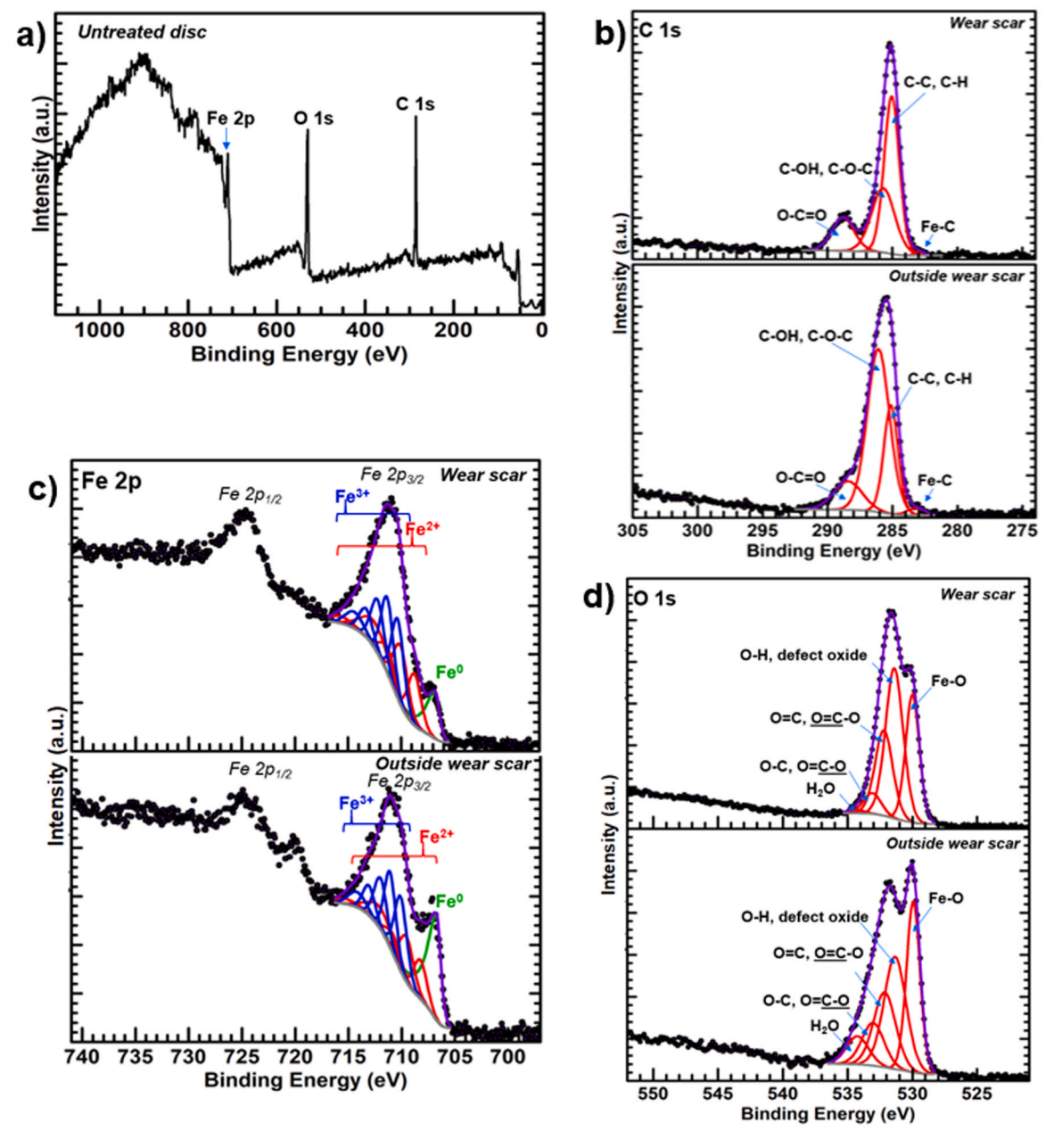
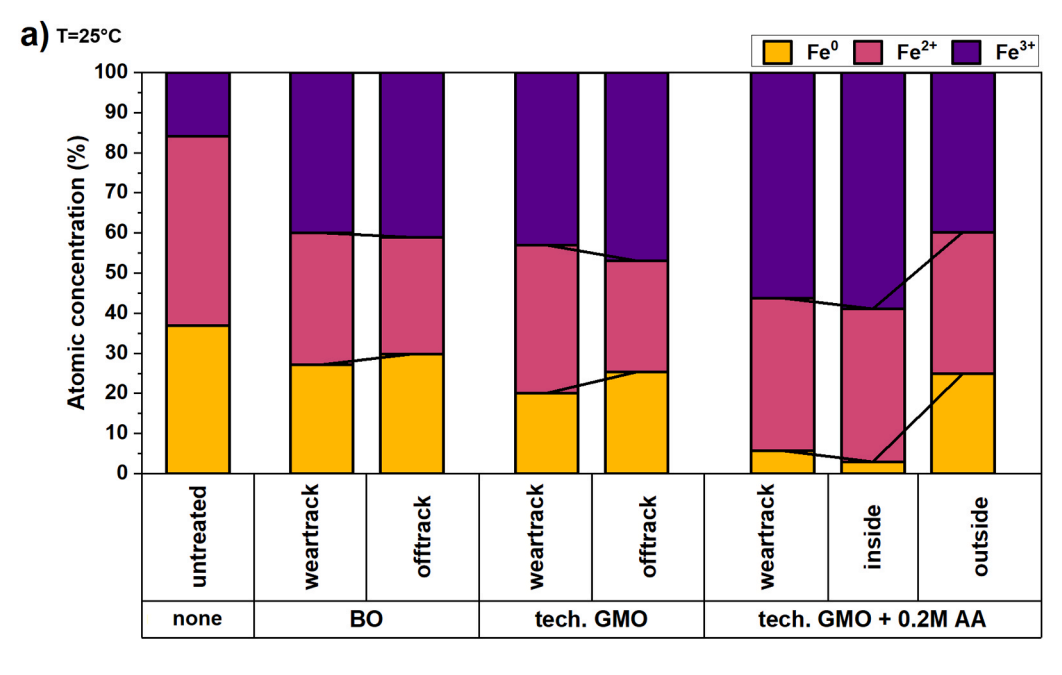


Fig. 6. XPS spectra: **a)** survey spectrum for untreated MTM disc, showing clear peaks for Fe 2p, O 1 s and C 1 s without other significant contributions. A weak peak around 350 eV corresponds to Ca 2p impurity. **b)** C 1 s, **c)** Fe 2p, and **d)** O 1 s XPS spectra for the wear track area and outside wear track area for the disc after tribotest in neat n-dodecane at 55°C as an example of the fit.

 μm [56]. Due to the heterogeneity of carbide regions, the intensity of its C 1 s emission depends on the measurement spot. In many cases, the Fe-C peak intensity was lower in the wear track than outside, which may suggest that the worn surface areas are covered with the newly formed oxide and organic overlayer. From C 1 s spectra only it is not possible to conclude which samples show the signs of chemisorption.

Fe $2p_{3/2}$ spectra (an example is presented in Fig. 6c) were fitted with one peak for metallic iron Fe 0 , 5 peaks for Fe $^{2+}$ and 5 peaks for Fe $^{3+}$ oxidation states, similarly to Molchan *et al.* [40]. The Fe 2p emission is complex due to presence of multiplets, and therefore it is impossible to directly link the peaks with the chemical species as for C 1 s and O 1 s. However, it remains an important source of information about the surface changes of the steel. Fe $2p_{1/2}$ was excluded from the fitting process altogether, as it overlaps with additional satellite peaks and does not substantially alter to the atomic concentration ratios derived from fitting

only the Fe $2p_{3/2}$ components. Clear trends for each fitted Fe species can be observed, though. Fe²⁺ (Fe₂O₃) and Fe³⁺ (Fe₃O₄ and FeOOH) contents as well as the ratio of Fe⁰/Fe²⁺/Fe³⁺ gives information about the oxides and hydroxides produced in the wear area. Atomic concentrations of Fe species are presented in Fig. 7a (at 25°C) and Fig. 8a (at 55°C) for formulations based on *n*-dodecane and in Fig. 9a on Yubase-4. In almost all cases, the metallic iron concentration decreases in the wear track compared to the outside area while the content of Fe²⁺ and Fe³⁺ increases, indicating the formation of an oxide layer in the tribocontact. Fe³⁺ content increases mostly in visibly corroded samples, after tests in lubricants containing acetic acid or water, *e.g.*, the disc after tech. GMO + 0.2 M AA at 25°C. For the neat base oil, more oxide is present in the wear track for the sample tested at 55°C compared to the one tested at 25°C, which can be explained by the thinner oil film, exposing the steel surfaces to direct contact and increasing wear. The changes in metallic



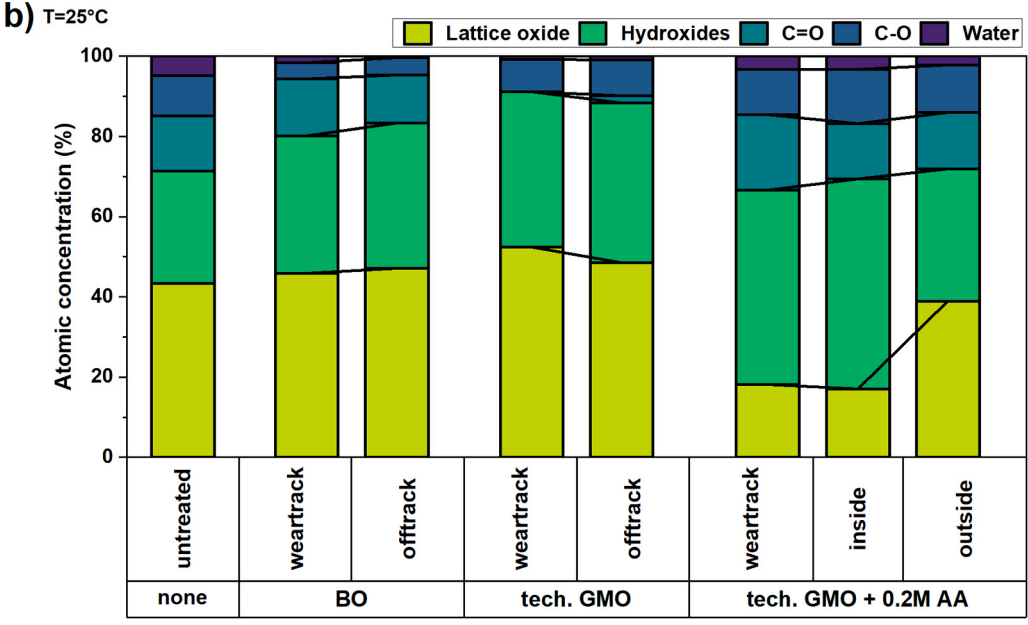


Fig. 7. Comparison of atomic concentration of a) combined iron components from Fe 2p spectra and b) oxygen components from O 1 s spectra for discs after tribotests in n-dodecane at 25°C. Tech. GMO + 0.2 AA was tested in 3 spots (explanation in the text). Not all tested samples could be measured by XPS due to magnetisation. 'None' in the first column means 'no lubricant'.

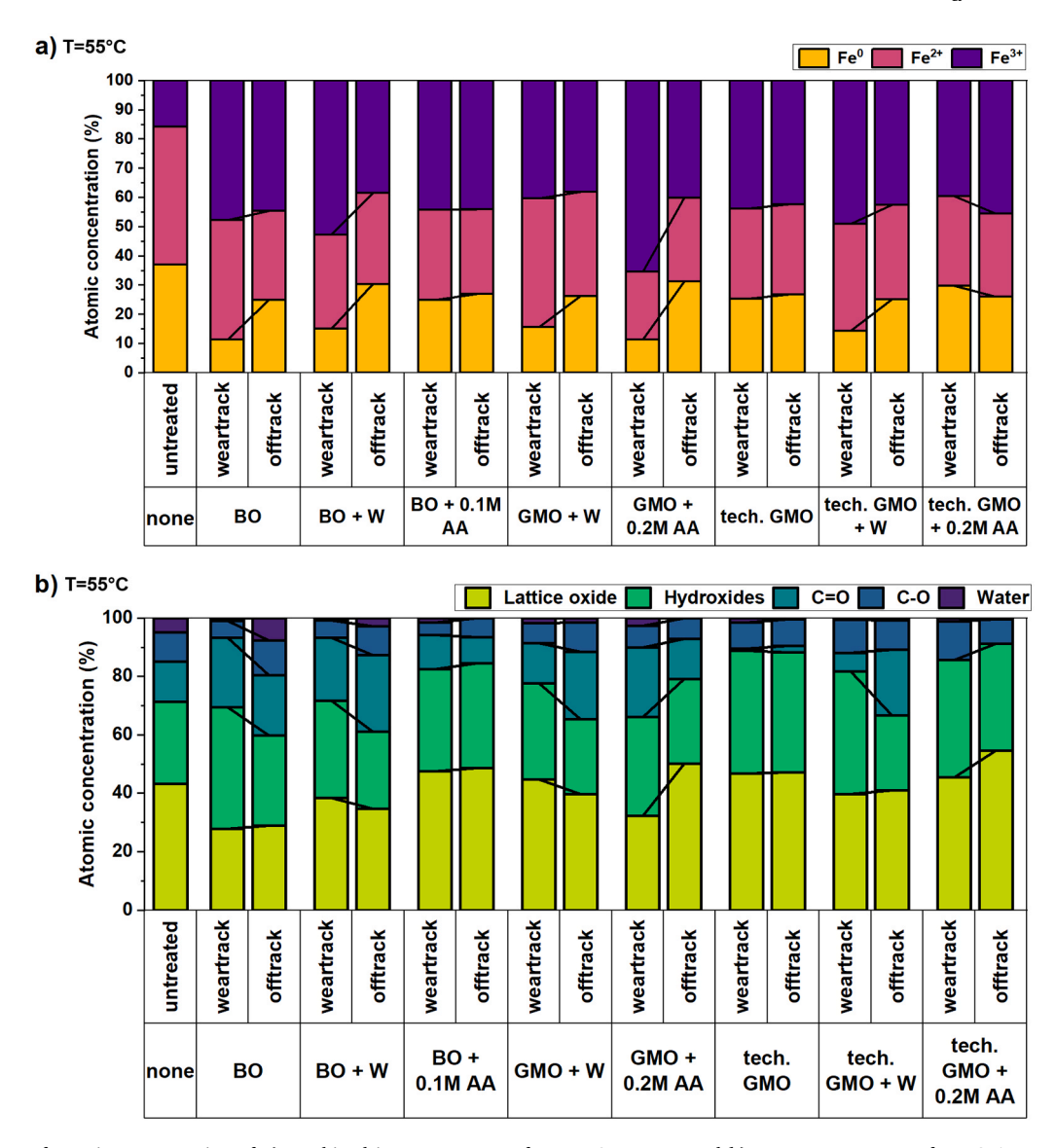


Fig. 8. Comparison of atomic concentration of **a**) combined iron components from Fe 2p spectra and **b**) oxygen components from O 1 s spectra for discs after tribotests in *n*-dodecane at **55**°C. Not all tested samples could be measured by XPS due to magnetisation. 'None' in the first column means 'no lubricant'.

content are also visible between the untreated sample and outside wear track area in all cases. It suggests that contact with the lubricant without friction already changes the steel surface (generally decreasing the ${\rm Fe^0}$ content and increasing ${\rm Fe^{2+}/Fe^{3+}}$), possibly due to the chemisorption occurring at elevated test temperature or during storing the discs with the residual oil film before the XPS measurement. In this case, comparing the spectra for the same sample in the wear track and away from it is essential for determining the effect of friction rather than comparing the untreated sample with tested discs. A useful indication of the level of friction-induced oxidation and chemical attack of the lubricant outside the tribocontact is the ${\rm Fe^{3+}}$ concentration ratio between the wear track and off-track area (Fig. S3 in the Supplementary Information).

In the O 1 s spectra (an example is presented in Figs. 6d), 5 main components were identified: main Fe-O oxide, defect oxide and hydroxides, 2 organic peaks [55,57] and 1 peak for water. Corresponding atomic concentrations are summarized in Fig. 7b and Fig. 8b for formulations in *n*-dodecane and in Fig. 9b for Yubase-4. The trend of increased hydroxide content in the wear track indicates corrosion and agrees with the Fe 2p data. Wear tracks of the samples tested in oils containing acid or water show a higher content of water than outside the

wear track. In the case of acid-containing formulations, the higher water content can arise from the corrosion redox reactions of steel. Moreover, higher water content is also observed for undoped tech. GMO samples, as the technical grade OFM is hygroscopic and contains water as received. Due to the difficult interpretation of C 1 s spectra, carbon-oxygen components from O 1s spectra were compared to approach the question of chemisorption and chemical changes of OFMs in the tribocontact. Assuming that OFMs adsorb through the free hydroxyl group, hydroxides content can also be ascribed to them. GMO, tech. GMO and AA have C=O group(s), and esters have C-O-C bonding, therefore, both organic peaks in O 1 s spectra should be considered in the analysis of adsorbed species. In Fig. 7b and Fig. 8b, C=O concentration indeed increased in the samples containing AA and/or GMO. In GMO + AA at both concentrations both molecules can contribute to the content of this component. Surprisingly, very low concentrations of C=O are observed for tech. GMO at both 25 and 55°C and tech. GMO + 0.2 M AA at 55 $^{\circ}$ C. Possibly the carbonyl group in the ester undergoes a tribochemical reaction, forming a better lubricating species that could chemisorb. This can explain higher concentrations of C-O species in these samples, as C-O can come from the reacted carbonyl group alongside the native C-O bond present in these molecules. For other

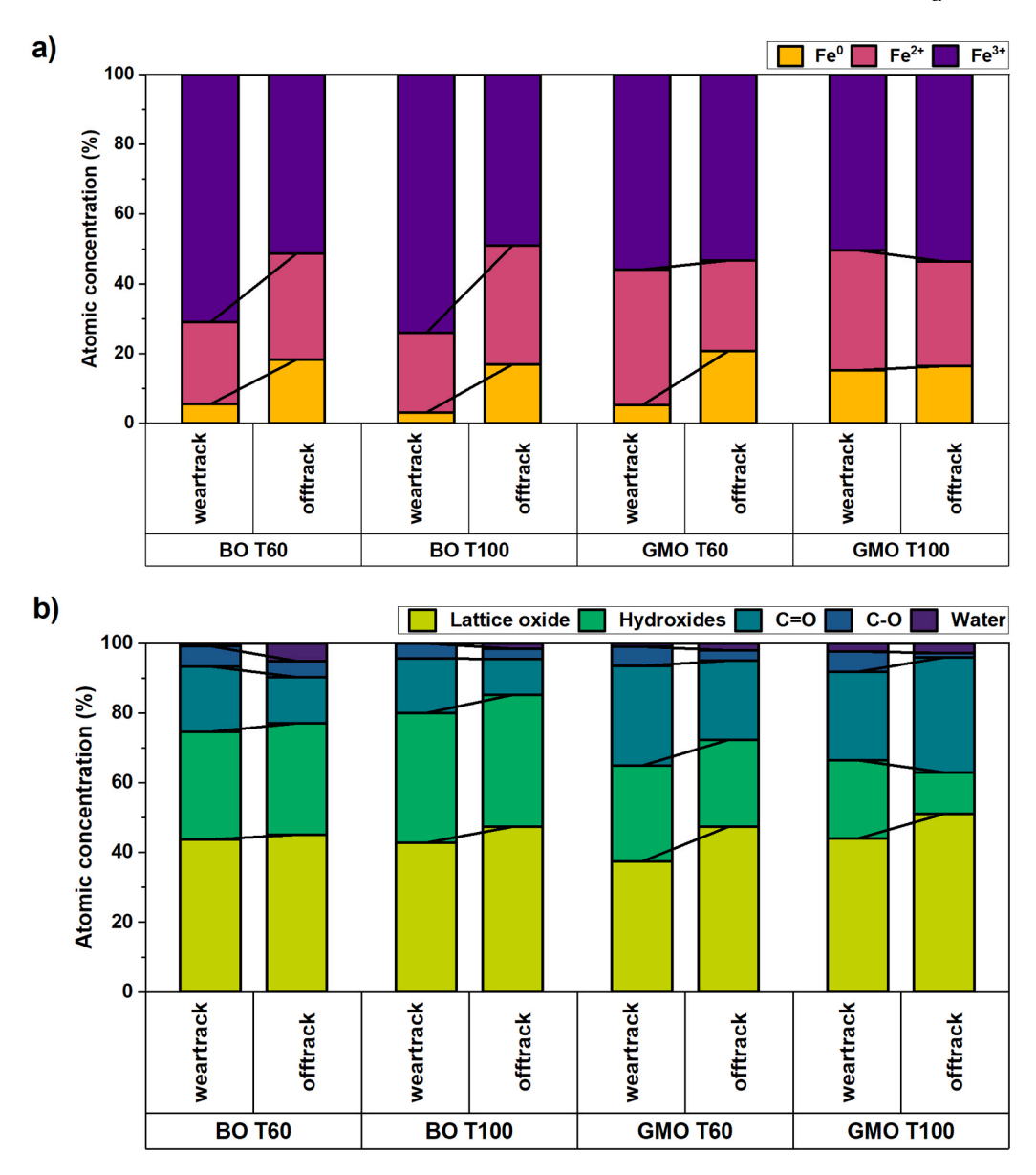


Fig. 9. Comparison of atomic concentration of a) combined iron components from Fe 2p spectra and b) oxygen components from O 1 s spectra for discs after tribotests in Yubase-4 at 60°C and 100°C (T60 and T100, respectively). Noisy spectra from the disc after the tech. GMO test at 60°C were excluded from the analysis.

samples, the C-O content is similar, comparing the wear track and off-track area and samples between each other. No clear trends between the two temperatures were noticed, because of the limited number of samples in the same oil formulations tested by XPS. Quantitative interpretation of the O 1 s spectra must be done with care, however, due to the combination of adsorbed and adventitious oxygen species [58] – as can be seen for untreated disc, all oxygen components were found on the surface.

The residual oil film was kept on the disc surfaces to prevent oxidation, especially of the wear track. However, leaving a small amount of the oil (especially acid-doped) could keep modifying the chemical composition of the surface. Despite no drastic change observed between the tribotest and XPS measurement (*i.e.*, visible corrosion was noticed just after the end of the MTM measurement of specific samples and it did not obviously progress outside the wear track area over 2 weeks), iron and oxygen species concentration can differ from those for the freshly tested sample.

To complement the spectroscopic study, a white light interferometer was used to collect 3D profiles of the samples tested in *n*-dodecane, from which roughness change or wear loss can be obtained. This non-

destructive technique was chosen over contact profilometry to avoid destroying the corroded layer and was well-suited for the reflective surfaces of the MTM discs. As the samples were tested shortly, mainly to collect Stribeck curves without prolonged rubbing, wear loss is not significant in most cases (but can give an insight into the early wear stages). An example of WLI 2D map 1D profiles for the disc after the test in tech. GMO + 0.2 M AA at $25^{\circ}\mathrm{C}$ is shown in Fig. 10. Mean wear track widths for all samples are collated in Fig. 11, together with wear track pictures obtained from Vision64 software. Noteworthy, in many cases, especially samples produced in the absence of polar small molecules, the wear track was unnoticeable by interferometry and had an assigned value of 0 mm.

Tech. $GMO+0.2\ M$ AA produced the widest wear track of all studied samples with visible signs of corrosion (red rust, 'inside' point in XPS), but the middle part of the track ('weartrack' in XPS) is only slightly rougher than the off-track area and in the picture, it looks almost unaffected. This can explain the very low traction coefficient for this formulation because the actual ball-disc contact shows no wear (Fig. 10), understood as the material loss and an indentation in the surface profile. Severe damage to the area next to the contact is caused

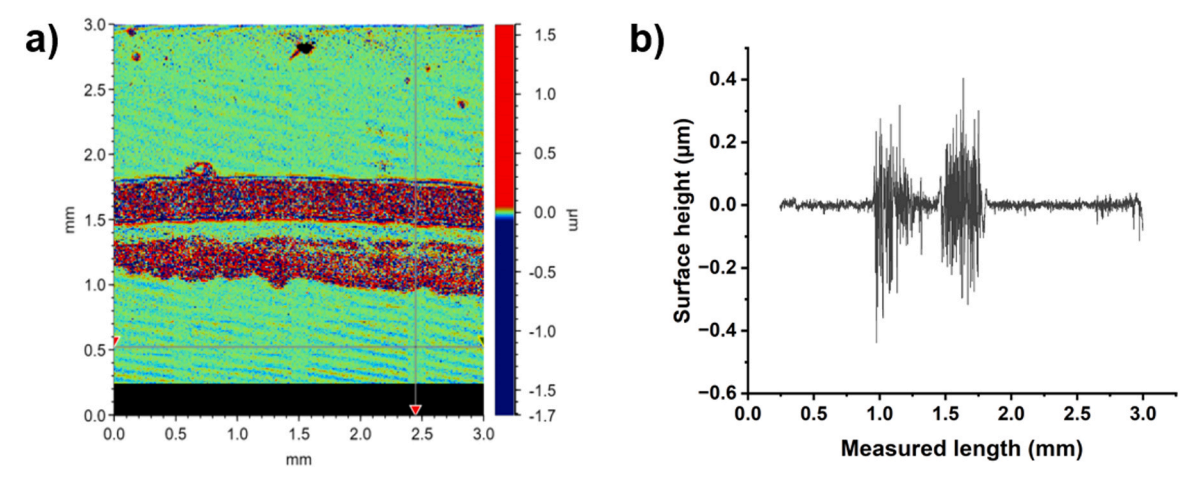


Fig. 10. An example result of WLI: a) 2D map and b) 1D profile along Y direction of tech. GMO + 0.2 M AA sample tested at 25°C showed severe wear outside the ball-disc contact and unaffected contact area (it has the same roughness as the rest of the surface).

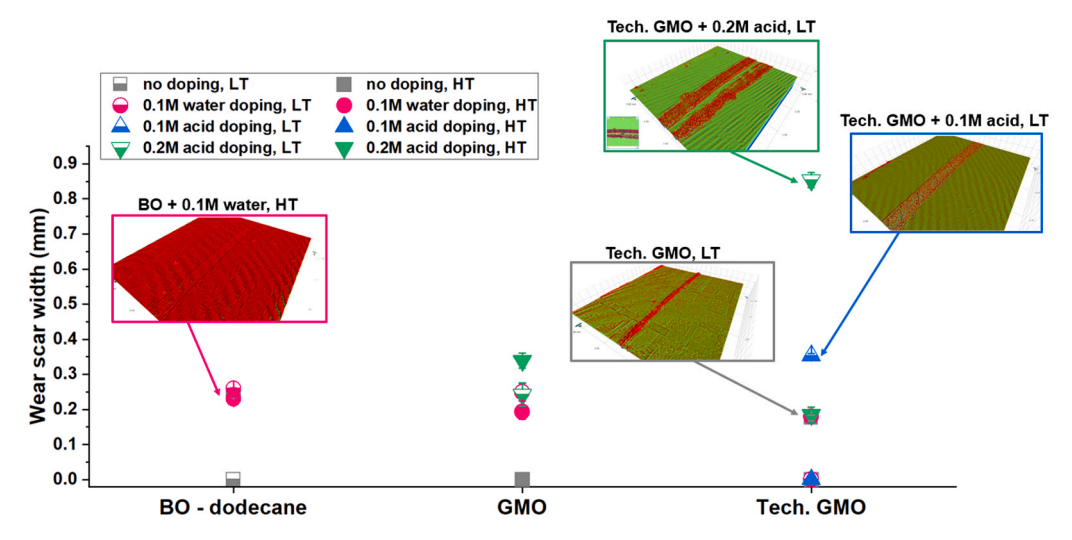


Fig. 11. Wear track widths for discs after tribotests in undoped and doped OFM solutions, obtained from WLI profiles. Interesting wear track profiles showing a wide range of possible morphologies are presented: (from the left) BO + 0.1 M water, HT - barely noticeable wear track; Tech. GMO + 0.2 M acid, LT - extensive wear track with the corroded border and smooth inside part; Tech. GMO, LT - well defined, narrow wear track; Tech. GMO + 0.1 M acid, LT - relatively wide wear track with defined border. Noteworthy, part of the samples produced no detectable wear track. LT - lower test temperature (25°C), HT - higher test temperature (55°C).

by acid, a standard corrosion agent for non-stainless steels. It can be suspected that due to the slide-to-roll ratio of 150 %, where both the ball and the disc are moving, the ball could constantly push out the part of the lubricant to the sides of the contact, creating locally a higher concentration of the acid than in the contact itself [59]. A small amount of residual water present in tech. GMO can also promote corrosion, but there is a lack of signs of this process in undoped tech. GMO sample (apart from the presence of water in XPS O 1 s spectra) means that the acid is mostly responsible. Comparing results from WLI and XPS for this sample, however, the atomic concentration of iron and oxygen species in the wear track and rusty area is more similar to each other than the wear track and off-track ('outside' point in XPS) area. The rust deposit is much rougher and higher than the native steel surface. Its absence in the direct disc-ball contact area while the chemical composition is similar suggests that the corrosion layer was formed and then removed during sliding-rolling contact because of low adhesion of the corroded material to the steel surface apart from the thin layer that stayed on the disc after the contact, and this removal process led to lower traction than in other tech. GMO-containing samples at 25°C. This is supported by the Fe³⁺ ratio (Fig. S3 in the Supplementary Information), which reaches 0.869. This is the lowest value from all tested samples, especially others with

 $0.2\ M$ AA addition and suggests that the bare steel surface was exposed in the wear track area.

Summarising XPS and WLI, in most cases for samples tested both in n-dodecane and Yubase-4 formulations, there is a noticeable difference between the area of disc-ball contact and outside of it. However, the relationship between the used lubricant, conditions of the test, wear and chemical composition is not trivial. Generally, if there was a visible wear track on the disc, the concentration of metallic iron in the contact decreased for the sake of increased Fe²⁺ and Fe³⁺ compared to the offtrack area, and the concentration of Fe³⁺ was higher for the samples with clear signs of corrosion. The Fe³⁺ ratio between the wear track and off-track area (Fig. S3 in the Supplementary Information) shows 63 % more Fe^{3+} species in the wear track than off-track for GMO + 0.2 M AA at 55°C sample and 48 % more for tech. GMO + 0.2 M AA at 25°C sample. The biggest differences in the species content from XPS and wear track widths were noted for tech. GMO, where the combination of esters and some contaminants leads to such a diverse response to friction when mixed with the base oil and polar molecules. Each component of the oil and its concentration matters, and better control over the content of glycerol mono-, di- and triester may further improve the friction reduction of this OFM (which is generally better than the pure GMO).

However, this would require modification in the synthesis process or making the mixture from the pure esters, which would dramatically increase the price of this additive.

Some samples, especially after tests at 25°C, could not be measured by XPS due to magnetisation leading to the disturbance of the photoelectron trajectories in electrostatic lenses of the used XPS system, resulting in substantial signal loss (XPS measurements in instruments with magnetic lenses are much less affected by sample magnetisation). Interestingly, all samples treated with GMO in *n*-dodecane at 25°C and with GMO formulations free from polar small molecule additives at 55°C displayed magnetism, which is not observed for the doped GMO oils at 55°C. Other samples that showed this effect and could not be measured were *n*-dodecane with water and tech. GMO with water. It suggests that GMO facilitates tribomagnetisation in lubricated contacts. Mishina's study [60] confirms that magnetisation can occur at the early stages of sliding and is not related to wear loss. On the other hand, Gao et al. [61] suggest that plastic deformation and wear track width in steel are related to the level of magnetisation. Our WLI data (Fig. 11) indicate that the track widths remain similar for all GMO samples. In another paper, Gao et al. [62] discuss the lubricated and non-lubricated contact, noting that the level of the tribomagnetic effect is higher for unlubricated contact because of the greater plastic deformation. However, no comparison between different lubricants was made. It is possible when the contact is lubricated by pure GMO-containing oils, more magnetite is generated, to the level effectively preventing the XPS measurement. The samples after tech. GMO oils (especially the highly corroded tech. GMO \pm 0.2 M AA at 25°C) and base oil could be measured. This may suggest that the combination of higher traction (higher chance of plastic deformation) and more hydroxyl groups (compared to tech. GMO and/or coming from water) leads to increased magnetite content. Magnetite particles can also be generated normally during the operation of bearings and can be filtered [63,64], but tribomagnetisation, depending on the oil formulation, requires more attention, especially considering the lubricant usage in electric vehicles, where changes in local magnetic field may affect the performance of the electric motor or other components.

3.3. Reverse Micelle Structure of OFMs in n-Dodecane

SAXS patterns for the freshly-prepared lubricants are presented in Fig. 12. GMO forms ellipsoid reverse micelles in the base oil, as observed previously by Armstrong et al. [44]. Adding water causes the swelling of the ellipsoidal micelle, which is also in agreement with the previous study. Water is a polar molecule and immiscible with dodecane, so to reduce unfavourable contact between water and dodecane, the water is encapsulated inside the micelle, and the system becomes a cloudy emulsion. Ellipsoid dimensions from the SAXS fitting are summarised in Table 5. Tech. GMO micelles are generally more elongated and have greater R_e . This suggests that di- and tri-esters with greater molecule size also take part in the formation of micelles, even with different polar head (here with fewer free hydroxyl groups). This remains in agreement with Nguyen et al. [65], where the mixture of GMO and oleic acid was studied. Slight swelling can be observed for the GMO doped with AA, but the effect is not as pronounced as for water. Micelles of GMO and tech. GMO with acetic acid are more elongated (when comparing the R_e/R_p ratio) than for water-free and water-containing formulations. A part of acetic acid is probably placed inside the micelle, and a part acts as a co-solvent. This can be supported by observing the behaviour of pure GMO solutions, where undoped ones are unstable and tend to separate from the liquid after prolonged time at room temperature while adding AA leads to the increased solubilisation of this OFM.

Fig. 12 shows the 1D SAXS profiles for the undoped and doped OFM solutions in n-dodecane. In the high-q region of all datasets (0.01 – 1 Å $^{-1}$), a simple ellipsoid model was used to model the data. Due to the low contrast between the OFM tails and the solvent, a core-shell model

Table 5SAXS fitting results: equatorial and polar radii of the ellipsoid micelle.

Formulation	R_e (Å)	R_p (Å)
GMO	18.049	7.361
GMO + 0.1 M water	27.140	18.689
GMO + 0.2 M AA	21.730	9.488
Tech. GMO	20.913	4.272
Tech. GMO $+$ 0.1 M water	31.746	16.904
Tech. GMO $+$ 0.2 M AA	28.382	3.742

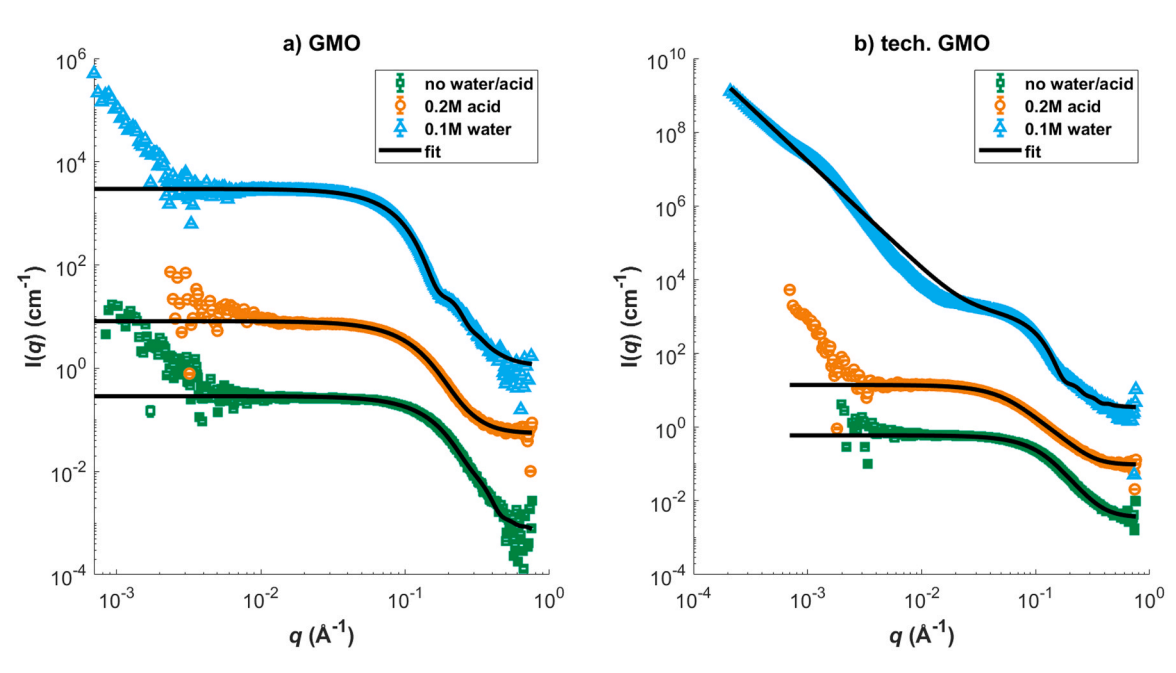


Fig. 12. 1D SAXS profiles from the undoped (green squares), acid-doped (orange circles) and water-doped (blue triangles) OFM solutions in *n*-dodecane and appropriate fits (black solid line), corresponding to the ellipsoidal form factor and the contribution of the power law in certain cases (see text). Plots are offset by a factor of 10 for clarity.

was not used here. For tech. GMO + 0.1 M water, the profile shows larger structures by the upturn in intensity in the low-q (> 0.01 Å $^{-1}$), not observed for GMO and undoped and acid-doped tech. GMO. The profile of tech. GMO + 0.1 M water was fitted using a combination of a power law to describe the low-q intensity and an ellipsoid model contributing to the broad peak in the high-q.

Despite the studied systems constituting largely nonaqueous media, the addition of a polar dopant, especially an acid, can lead to the protonation of the OFM. Although in nonpolar solvents such as n-dodecane, acid molecules cannot easily dissociate and will more likely aggregate, the used molar excess of the acid reacts with the OFM molecules. Although esters can be protonated in the presence of acid, no signs of such behaviour were found in pure GMO and tech. GMO doped with AA. The profile of tech. GMO + 0.1 M water shows modulation (fitted by power law only) likely due to a big water droplet entrapped in glycerol di- or trioleate aggregates. However, SAXS gives general, average information of the system, so the presence of this modulation in the profile shows a meaningful number of such aggregates rather than a single occurrence.

3.4. Proposed mechanism of friction reduction

As a summary of the presented data on lubricated contact (MTM), surface change (XPS, WLI) and bulk oil properties (SAXS), we propose the following mechanism of the friction reduction in the contact lubricated by the oil containing OFM and the polar small molecules.

The steel-lubricant interface promotes the adsorption of both the OFM and the polar small molecules. However, due to the higher polarity and smaller sizes of the latter, they adsorb first, followed by the amphiphilic OFM molecules. In the oil phase, OFM micelles are present and remain in equilibrium with the adsorbed layer, not excluding complex multilayer/colloidal adsorption layers, especially in prolonged steel-lubricant contact. Importantly, the self-assembly appears in the system without friction. Water also adsorbs preferentially to the steel surface, but more severely affects the equilibrium of the formulation, leading to precipitation of pure GMO in metastable phases. However, the OFM entraps water inside the micelle, facilitating the transfer of this polar component to the surface. No severe effect on the traction coefficient was noticed for freshly prepared water-doped formulations, but in such oils, phase separation will likely occur after an extended time or immediately at higher water concentration.

The friction reduction depends on the stability and thickness of the lubrication film. Therefore, more strongly adsorbed layers will lead to a lower traction coefficient. Acid-containing formulations at lower temperatures show extremely low traction coefficient but also severe wear around the contact due to a chemical attack of the acid on the steel, forming a rougher and more polar interface, further attracting the OFM molecules and creating an area for low-friction slip planes. In tech. GMO formulations, large molecules of glycerol di- and trioleate can form denser slip planes, because one adsorbed molecule (one polar head) is equivalent to two or three alkyl chains, which explains the lower traction coefficient for tech. GMO than for pure GMO, where one polar head corresponds to only one alkyl chain. Additionally, the carbonyl group (C=O) in esters may react under the tribocontact, chemisorbing to the steel rather than just adsorbing physically. Friction-induced reactions in different formulations lead to the generation of a specific oxidation layer, where the content of magnetite can vary. This substantially affects the magnetic properties of the whole sample to the point of preventing the XPS measurement and can result in disruption of operation in electric vehicles for example.

Therefore, for the effective operation of OFM, one must consider both the structure of the polar head and nonpolar chain(s) and the possible presence and nature of polar molecules that can be introduced into the oil from the external and the internal lubricant environment.

4. Conclusions

We have investigated the tribological properties of the model and industrial organic friction modifier in a commercial and model base oil, and for the model base oil formulations – also in the presence and absence of small molecule polar dopants that can appear in the lubricant during its lifetime. SAXS studies of the bulk oil were coupled with tribotests to better understand the structural changes in the lubricant upon doping.

From the presented data, it can be concluded that small polar molecules can affect lubrication by changing the self-assembly and adsorption of OFMs onto the steel surface. Both the type and concentration of the small molecules are important factors in reducing friction and must be considered together with the operating temperature and the choice of OFM. Water tends to enter the micelles of OFMs in the oil phase, increasing not only micellar dimensions but also enhancing the separation of pure GMO out of the oil at room temperature. However, contrary to the general idea that water presence disrupts the performance of the lubricant, in this study the 5 times higher concentration of water than the OFM almost does not affect the traction reduction of OFM-containing oils. Acetic acid stabilizes the oils by increasing the solubility of OFMs. The changes in traction coefficient are explained by improved adsorption of ester molecules in the presence of acid. High acid concentration decreases the traction coefficient of all studied formulations at 25°C but severe corrosion can occur. The level of wear and corrosion can be successfully examined by wear track morphology (from white light interferometry) and Fe 2p_{3/2} XPS spectra, coupled with O 1 s spectra. Highly corroded steel discs show a large increase of Fe³⁺ and hydroxide species in the wear track area and a constantly removed corroded layer also reduces friction, explaining the low traction coefficient in samples showing substantial wear and corrosion. Tribomagnetisation in pure GMO samples was highlighted, relating the structure of this OFM with the promoted formation of magnetite.

The observations presented here shed more light on the fundamental structure-performance relationships of OFMs in the presence of polar agents that can naturally appear in the lubricant during its lifetime. A controlled polar molecule doping of OFM-containing formulations to improve their friction-reducing properties is an attractive solution for more sustainable lubrication.

Statement of originality

We declare that this manuscript is the authors' original work, and has not already been published nor submitted simultaneously elsewhere. The manuscript has been approved by all authors.

CRediT authorship contribution statement

Andrew J. Britton: Investigation, Data curation. Lauren Matthews: Writing – review & editing, Investigation, Formal analysis. Camille Hammersley: Investigation, Data curation. Elizabeth A. Willneff: Supervision, Investigation, Formal analysis. Schroeder Sven L. M.: Writing – original draft, Supervision, Resources, Methodology, Funding acquisition, Conceptualization. Kicior Inga Urszula: Writing – original draft, Visualization, Methodology, Investigation, Formal analysis, Conceptualization. Ardian Morina: Writing – review & editing, Supervision, Resources, Conceptualization. Veijo Honkimäki: Supervision, Funding acquisition. Peter J. Dowding: Supervision, Resources, Funding acquisition, Conceptualization.

Declaration of Competing Interest

The authors declare that they have no known competing financial interests or personal relationships that could have appeared to influence the work reported in this paper.

Acknowledgements

We acknowledge the European Synchrotron Radiation Facility (ESRF) for the provision of synchrotron beamtime. I.K. acknowledges InnovaXN (European Union's Horizon 2020 research and innovation programme under the Marie Skłodowska-Curie grant agreement no. 847439) and Infineum UK Ltd. for funding. We acknowledge support from the Henry Royce Institute (EPSRC grants: EP/P022464/1, EP/R00661X/1), which funded the VXSF Facilities (https://engineering.leeds.ac.uk/vxsf) within the Bragg Centre for Materials Research at Leeds. SLMS acknowledges the support of the Bragg Centenary Chair by the Royal Academy of Engineering, Infineum UK Ltd., and Diamond Light Source. All data supporting this study are provided either in the results section of this paper or in the electronic supplementary information accompanying it.

Appendix A. Supporting information

Supplementary data associated with this article can be found in the online version at doi:10.1016/j.triboint.2025.111140.

Data availability

All data supporting this study are provided either in the results section of this paper or in the electronic supplementary information accompanying it.

References

- Wakabayashi T, Inasaki I. Function of cutting fluids and lubricants. Encyclopedia of Tribology. Boston, MA: Springer US; 2013. p. 1424

 –8. https://doi.org/10.1007/ 078.0.387.03897.5 1202
- [2] Hu C, You G, Liu J, Du S, Zhao X, Wu S. Study on the mechanisms of the lubricating oil antioxidants: experimental and molecular simulation. J Mol Liq 2021;324: 115099. https://doi.org/10.1016/j.molliq.2020.115099.
- [3] Spikes H. Friction modifier additives. Tribol Lett 2015;60:5. https://doi.org/ 10.1007/s11249-015-0589-z
- [4] Holmberg K, Erdemir A. Influence of tribology on global energy consumption, costs and emissions. Friction 2017;5:263–84. https://doi.org/10.1007/s40544-017-0183-5.
- [5] Spikes H. The history and mechanisms of ZDDP. Tribol Lett 2004;17:469–89. https://doi.org/10.1023/B:TRIL.0000044495.26882.b5.
- [6] Wong VW, Tung SC. Overview of automotive engine friction and reduction trends–Effects of surface, material, and lubricant-additive technologies. Friction 2016;4:1–28. https://doi.org/10.1007/s40544-016-0107-9.
- [7] Chen Y, Jha S, Raut A, Zhang W, Liang H. Performance characteristics of lubricants in electric and hybrid vehicles: a review of current and future needs. Front Mech Eng 2020;6. https://doi.org/10.3389/fmech.2020.571464.
- [8] Birleanu C, Pustan M, Cioaza M, Molea A, Popa F, Contiu G. Effect of TiO2 nanoparticles on the tribological properties of lubricating oil: an experimental investigation. Sci Rep 2022;12:5201. https://doi.org/10.1038/s41598-022-09245-
- [9] Shahnazar S, Bagheri S, Abd Hamid SB. Enhancing lubricant properties by nanoparticle additives. Int J Hydrog Energy 2016;41:3153–70. https://doi.org/ 10.1016/j.ijhydene.2015.12.040.
- [10] Ratoi M, Niste VB, Zekonyte J. WS2 nanoparticles potential replacement for ZDDP and friction modifier additives. RSC Adv 2014;4:21238–45. https://doi.org/ 10.1039/C4RA01795A
- [11] Wang B, Qiu F, Barber GC, Zou Q, Wang J, Guo S, et al. Role of nano-sized materials as lubricant additives in friction and wear reduction: a review. 204206 Wear 2022;490–1. https://doi.org/10.1016/j.wear.2021.204206.
- [12] Kossoko NF, Dubreuil F, Thiébaut B, Belin M, Minfray C. Diblock polymeric friction modifier (PFM) in the boundary regime: tribological conditions leading to low friction. Tribol Int 2021;163:107186. https://doi.org/10.1016/j. triboint.2021.107186.
- [13] Gmür TA, Mandal J, Cayer-Barrioz J, Spencer ND. Towards a Polymer-Brush-Based friction modifier for oil. Tribol Lett 2021;69:124. https://doi.org/10.1007/s11249-021-01496-w.
- [14] Cyriac F, Tee XY, Chow PS. Tribological performance of polymeric friction modifiers under sliding rolling contact condition. Lubr Sci 2024;36:119–34. https://doi.org/10.1002/ls.1678.
- [15] Delamarre S, Gmür T, Spencer ND, Cayer-Barrioz J. Polymeric friction modifiers: influence of anchoring chemistry on their adsorption and effectiveness. Langmuir 2022;38:11451–8. https://doi.org/10.1021/acs.langmuir.2c01782.
- [16] Stevens MC, Taylor NM, Guo X, Hussain H, Mahmoudi N, Cattoz BN, et al. Diblock bottlebrush polymer in a non-polar medium: Self-assembly, surface forces, and

- superlubricity. J Colloid Interface Sci 2024;658:639–47. https://doi.org/10.1016/
- [17] Straiton AndrewJ, Kathyola ThokozileA, Sweeney Callum, Parish JD, Willneff EA, Schroeder SvenL M, et al. Green alternatives to zinc dialkyldithiophosphates: vanadium Oxide-Based additives. ACS Appl Eng Mater 2023;1:2916–25. https://doi.org/10.1021/acsaenm.3c00425.
- [18] Jiménez A-E, Avilés M-D, Pamies R, Bermúdez M-D, Carrión-Vilches F-J, Sanes J. Ecofriendly protic ionic liquid lubricants for Ti6Al4V. Lubricants 2022;11:5. https://doi.org/10.3390/lubricants11010005.
- [19] Avilés MD, Carrión FJ, Sanes J, Bermúdez MD. Bio-based ionic liquid crystal for stainless steel-sapphire high temperature ultralow friction. 204020 Wear 2021: 484–5. https://doi.org/10.1016/j.wear.2021.204020.
- [20] Zhou Y, Qu J. Ionic liquids as lubricant additives: a review. ACS Appl Mater Interfaces 2017;9:3209–22. https://doi.org/10.1021/acsami.6b12489.
- [21] Khanmohammadi H, Wijanarko W, Espallargas N. Ionic liquids as additives in Water-Based lubricants: from surface adsorption to tribofilm formation. Tribol Lett 2020;68:130. https://doi.org/10.1007/s11249-020-01377-8.
- [22] Campen SM. Fundamentals of organic friction modifier behaviour. Imperial College London; 2012.
- [23] Hu M, Ma R, Zhang S, Han Y, Zhao J, Zhang M, et al. Preparation and tribological study of novel amide-based organic friction modifiers. Tribol Int 2024;194:109465. https://doi.org/10.1016/j.triboint.2024.109465.
- [24] Cyriac F, Tee XY, Poornachary SK, Chow PS. Influence of structural factors on the tribological performance of organic friction modifiers. Friction 2021;9:380–400. https://doi.org/10.1007/s40544-020-0385-0.
- [25] Zachariah Z, Nalam PC, Ravindra A, Raju A, Mohanlal A, Wang K, et al. Correlation between the adsorption and the nanotribological performance of fatty Acid-Based organic friction modifiers on stainless steel. Tribol Lett 2020;68:11. https://doi. org/10.1007/s11249-019-1250-z.
- [26] Yi X, Xu H, Jin G, Lu Y, Chen B, Xu S, et al. Boundary slip and lubrication mechanisms of organic friction modifiers with effect of surface moisture. Friction 2024. https://doi.org/10.1007/s40544-023-0820-0.
- [27] Fry BM, Moody G, Spikes HA, Wong JSS. Adsorption of organic friction modifier additives. Langmuir 2020;36:1147–55. https://doi.org/10.1021/acs. langmuir.9b03668.
- [28] Shrestha LK, Glatter O, Aramaki K. Structure of nonionic surfactant (Glycerol α-Monomyristate) micelles in organic solvents: a SAXS study. J Phys Chem B 2009; 113:6290–8. https://doi.org/10.1021/jp900102e.
- [29] Shrestha LK, Shrestha RG, Abe M, Ariga K. Reverse micelle microstructural transformations induced by oil and water. Soft Matter 2011;7:10017. https://doi. org/10.1039/clsm06047c.
- [30] Shrestha RG, Shrestha LK, Acharya S, Aramaki K. Water induced microstructure transformation of diglycerol monolaurate reverse micelles in ethylbenzene. J Oleo Sci 2012;61:575–84. https://doi.org/10.5650/jos.61.575.
- [31] Bradley-Shaw JL, Camp PJ, Dowding PJ, Lewtas K. Glycerol monooleate reverse micelles in nonpolar solvents: computer simulations and Small-Angle neutron scattering. J Phys Chem B 2015;119:4321–31. https://doi.org/10.1021/acs. incb 5b00213
- [32] Bradley-Shaw JL, Camp PJ, Dowding PJ, Lewtas K. Molecular dynamics simulations of glycerol monooleate confined between mica surfaces. Langmuir 2016;32:7707–18. https://doi.org/10.1021/acs.langmuir.6b00091.
- [33] Vuorte M, Kuitunen S, Van Tassel PR, Sammalkorpi M. Equilibrium state model for surfactants in oils: colloidal assembly and adsorption. J Colloid Interface Sci 2023; 630:783–94. https://doi.org/10.1016/j.icis.2022.09.153.
- [34] Cyriac F, Lugt PM, Bosman R, Venner CH. Impact of water on EHL film thickness of lubricating greases in rolling point contacts. Tribol Lett 2016;61:23. https://doi. org/10.1007/s11249-016-0642-6.
- [35] Lancaster JK. A review of the influence of environmental humidity and water on friction, lubrication and wear. Tribol Int 1990;23:371–89. https://doi.org/ 10.1016/0301-679X(90)90053-R.
- [36] Besser C, Steinschütz K, Dörr N, Novotny-Farkas F, Allmaier G. Impact of engine oil degradation on wear and corrosion caused by acetic acid evaluated by chassis dynamometer bench tests. Wear 2014;317:64–76. https://doi.org/10.1016/j. wear.2014.05.005.
- [37] Costa HL, Cousseau T, Souza RM. Current knowledge on friction, lubrication, and wear of Ethanol-Fuelled Engines—A review. Lubricants 2023;11:292. https://doi. org/10.3390/lubricants11070292.
- [38] AZOMaterials. AISI 52100 Alloy Steel (UNS G52986) n.d.
- [39] Biesinger MC, Payne BP, Grosvenor AP, Lau LWM, Gerson AR, Smart. RStC. resolving surface chemical states in XPS analysis of first row transition metals, oxides and hydroxides: cr, mn, fe, co and ni. Appl Surf Sci 2011;257:2717–30. https://doi.org/10.1016/j.apsusc.2010.10.051.
- [40] Molchan IS, Thompson GE, Skeldon P, Lindsay R, Walton J, Kouvelos E, et al. Microscopic study of the corrosion behaviour of mild steel in ionic liquids for CO 2 capture applications. RSC Adv 2015;5:35181–94. https://doi.org/10.1039/ CSR401007G
- [41] Omran M, Fabritius T, Elmahdy AM, Abdel-Khalek NA, El-Aref M, Elmanawi AE-H. XPS and FTIR spectroscopic study on microwave treated high phosphorus iron ore. Appl Surf Sci 2015;345:127–40. https://doi.org/10.1016/j.apsusc.2015.03.209.
- [42] Kousar K, Dowhyj M, Walczak MS, Ljungdahl T, Wetzel A, Oskarsson H, et al. Corrosion inhibition in acidic environments: key interfacial insights with photoelectron spectroscopy. Faraday Discuss 2022;236:374–88. https://doi.org/ 10.1039/D1FD00106J.
- [43] YUBASE 4 Safety Data Sheet. 2023.
- [44] Armstrong AJ, Apóstolo RFG, McCoy TM, Allen FJ, Doutch J, Cattoz BN, et al. Experimental and simulation study of self-assembly and adsorption of glycerol

- monooleate in n -dodecane with varying water content onto iron oxide. Nanoscale 2024;16:1952–70. https://doi.org/10.1039/D3NR05080G.
- [45] Armstrong AJ, McCoy TM, Welbourn RJL, Barker R, Rawle JL, Cattoz B, et al. Towards a neutron and X-ray reflectometry environment for the study of solid-liquid interfaces under shear. Sci Rep 2021;11:1–12. https://doi.org/ 10.1038/s41598-021-89189-1.
- [46] Fry BM, Chui MY, Moody G, Wong JSS. Interactions between organic friction modifier additives. Tribol Int 2020;151:106438. https://doi.org/10.1016/j. triboint.2020.106438.
- [47] Hamrock BJ, Dowson D. Isothermal elastohydrodybamic Lubr Point Contacts 1976.
- [48] Chittenden RJ, Dowson D, Dunn JF, Taylor CM. A theoretical analysis of the isothermal elastohydrodynamic lubrication of concentrated contacts. I. direction of lubricant entrainment coincident with the major axis of the hertzian contact ellipse. Proc R Soc Lond A Math Phys Sci 1985;397:245–69. https://doi.org/ 10.1098/rspa.1985.0014.
- [49] Welinder BS, Sørensen HH. Alternative mobile phases for the reversed-phase high-performance liquid chromatography of peptides and proteins. J Chromatogr A 1991;537:181–99. https://doi.org/10.1016/S0021-9673(01)88894-4.
- [50] Subirats X, Casanovas L, Redón L, Rosés M. Effect of the solvent on the chromatographic selectivity in reversed-phase and HILIC. Adv Sample Prep 2023;6: 100063. https://doi.org/10.1016/j.sampre.2023.100063.
- [51] Tjahjono M, Allian AD, Garland M. Experimental dipole moments for nonisolatable acetic acid structures in a nonpolar medium. A combined spectroscopic, dielectric, and DFT study for Self-Association in solution. J Phys Chem B 2008;112:6448–59. https://doi.org/10.1021/jp800609w.
- [52] Clough SA, Beers Y, Klein GP, Rothman LS. Dipole moment of water from stark measurements of H2O, HDO, and D2O. J Chem Phys 1973;59:2254–9. https://doi. org/10.1063/1.1680328.
- [53] Shi J, Zhou Q, Sun K, Liu G, Zhou F. Understanding adsorption behaviors of organic friction modifiers on hydroxylated SiO 2 (001) surfaces: effects of molecular polarity and temperature. Langmuir 2020;36:8543–53. https://doi.org/10.1021/ acs.langmuir.0c01386.
- [54] Wang W, Shen B, Li Y, Ni Q, Zhou L, Du F. Friction reduction mechanism of glycerol monooleate-containing lubricants at elevated temperature - transition from physisorption to chemisorption. Sci Prog 2021;104:1–15. https://doi.org/ 10.1177/0036850421998529.

- [55] Long Y, Bouchet M-IDB, Lubrecht T, Onodera T, Martin JM. Superlubricity of glycerol by self-sustained chemical polishing. Sci Rep 2019;9:6286. https://doi. org/10.1038/s41598-019-42730-9.
- [56] Ravi G, Daems P-J, Nikolic K, De Waele W, Helsen J, Petrov R, et al. An interdisciplinary framework to predict premature roller element bearing failures in wind turbine gearboxes. Forsch Ing 2021;85:229–40. https://doi.org/10.1007/ s10010-021-00463-0.
- [57] Minfray C, Le Mogne T, Martin J-M, Onodera T, Nara S, Takahashi S, et al. Experimental and molecular dynamics simulations of tribochemical reactions with ZDDP: zinc Phosphate–Iron oxide reaction. Tribology Trans 2008;51:589–601. https://doi.org/10.1080/10402000802011737.
- [58] Kousar K, Walczak MS, Ljungdahl T, Wetzel A, Oskarsson H, Restuccia P, et al. Corrosion inhibition of carbon steel in hydrochloric acid: elucidating the performance of an imidazoline-based surfactant. Corros Sci 2021;180:109195. https://doi.org/10.1016/j.corsci.2020.109195.
- [59] Tomala A, Naveira Suarez A, Rodríguez Ripoll M. Tribological behaviour of corrosion inhibitors in metal working fluids under different contact conditions. 347–56 Adv Mat Res 2014:966–7. https://doi.org/10.4028/www.scientific.net/ AMR 966-967 347
- [60] Mishina H. Magnetization of ferromagnetic material surfaces by tribological process. J Appl Phys 2002;92:6721–7. https://doi.org/10.1063/1.1519340.
- [61] Gao F, Fan J, Zhang L, Chen B. Unraveling the origin of tribomagnetization in ferromagnetic materials. ACS Appl Mater Interfaces 2020;12:50176–86. https://doi.org/10.1021/acsami.0c15044.
- [62] Gao F, Fan J, Zhang L, Jiang J, He S. The generation of the tribo-magnetization in a ferromagnetic material during the friction process. J Magn Magn Mater 2020;493: 165741. https://doi.org/10.1016/j.jmmm.2019.165741.
- [63] Nilsson R, Olofsson U, Sundvall K. Filtration and coating effects on self-generated particle wear in boundary lubricated roller bearings. Tribol Int 2005;38:145–50. https://doi.org/10.1016/j.triboint.2004.07.022.
- [64] Menzel K, Lindner J, Nirschl H. Removal of magnetite particles and lubricant contamination from viscous oil by High-Gradient magnetic separation technique. Sep Purif Technol 2012;92:122–8. https://doi.org/10.1016/j.seppur.2011.07.035.
- [65] Nguyen NA, Liu DY, Krogstad DV. Impact of water and oleic acid on glycerol monooleate phase transition and bi-continuous structure formation in White oil. Soft Matter 2024;20:7237–45. https://doi.org/10.1039/D4SM00809J.